

Effect of a magnetic field on the two-phonon Raman scattering in graphene

C. Faugeras,¹ P. Kossacki,^{1,2} D. M. Basko,³ M. Amado,^{1,4}
M. Sprinkle,⁵ C. Berger,^{5,6} W.A. de Heer,⁵ and M. Potemski¹

¹LNCMI-CNRS, BP 166, 38042 Grenoble, France

²Institute of Experimental Physics, University of Warsaw, Poland

³Laboratoire de Physique et Modélisation des Milieux Condensés,
Université Joseph Fourier and CNRS, 25 rue des Martyrs, 38042 Grenoble, France

⁴QNS-GISC, Departamento de Física de Materiales,
Universidad Complutense, E-28040 Madrid, Spain

⁵School of Physics, Georgia Institute of Technology, Atlanta, Georgia 30332, USA

⁶CNRS-Institut Néel, BP 166, 38042 Grenoble Cedex 9, France.

We have studied, both experimentally and theoretically, the change of the so-called $2D$ band of the Raman scattering spectrum of graphene (the two-phonon peak near 2700 cm^{-1}) in an external magnetic field applied perpendicular to the graphene crystal plane at liquid helium temperature. A shift to lower frequency and broadening of this band is observed as the magnetic field is increased from 0 to 33 T. At fields up to 5–10 T the changes are quadratic in the field while they become linear at higher magnetic fields. This effect is explained by the curving of the quasiclassical trajectories of the photo-excited electrons and holes in the magnetic field, which enables us (i) to extract the electron inelastic scattering rate, and (ii) to conclude that electronic scattering accounts for about half of the measured width of the $2D$ peak.

PACS numbers: 63.22.+m, 63.20.Kr, 78.30.Na, 78.67.-n

I. INTRODUCTION

Graphene, a two-dimensional plane of carbon atoms arranged in a honeycomb lattice, has stimulated many experimental and theoretical efforts to study and understand its exotic electronic and optical properties¹. Graphene can be produced by mechanical exfoliation of bulk graphite², by the decomposition of a SiC substrate at high temperatures³ or by epitaxial growth on different metal surfaces⁴. Graphene on SiC is well adapted for optical measurements as samples are of macroscopic size and lie on a substrate which can be insulating, and hence, transparent in a wide, from far-infrared to visible spectral range.

Raman scattering is a key element to graphene studies as it is a reliable and non-destructive technique to establish the monolayer character of a graphene specimen^{5,6} or the negligible interlayer coupling in multilayer epitaxial graphene (MEG) samples⁷. This relies on the analysis of the shape of the observed $2D$ band feature (the two-phonon peak around 2700 cm^{-1} , also referred as D^* or G') which is the second-order overtone of the D band. While defects (in a general meaning – impurities, interface roughness, etc.) are needed for the D band to be observed, the $2D$ band is always seen and it even appears as the most pronounced feature in the Raman scattering spectrum of graphene. Because of the doubly-resonant nature of the D band^{8,9} and the fully-resonant nature of the $2D$ band,^{10,11} they both show a dispersive behavior with the excitation energy, what allowed to tracing the phonon band structure of different carbon allotropes^{12,13}. In this paper, we show that a strong magnetic field applied perpendicular to the plane of a graphene crystal significantly affects the $2D$ band feature. Increasing the

magnetic field up to 33 T, we observe a simultaneous red shift of the $2D$ band energy and a strong broadening of the peak.

In the following, we show that the evolution of the $2D$ band in magnetic field can be understood and modelled quantitatively as a pure orbital effect of the magnetic field on the intermediate states of the Raman process, i. e., electrons and holes. The field induces circular orbits to the photo-generated electron-hole pairs, and this modifies the momenta of the optical phonons emitted during the Raman scattering process. This leads to a red shift and to a broadening of the $2D$ band feature as the magnetic field is increased, an effect that we observe experimentally and describe theoretically below. We note that this effect is not specific to a graphene monolayer as the two essential ingredients are the fully-resonant nature of the $2D$ peak, and the free motion of electrons in the plane. Thus, it should also be characteristic for the multilayer graphene and graphite.

II. SAMPLES AND EXPERIMENT

Raman scattering measurements were performed in the backscattering geometry at liquid helium temperature and in magnetic fields up to 33 T applied perpendicular to the plane of the graphene crystal. A Ti:Sapphire laser tuned at an accurately controlled wavelength of 720 nm (corresponding to the incident photon energy $\hbar\omega_{\text{in}} = 1.722\text{ eV}$) was used for excitation. Optical fibers, both with a core diameter of $200\text{ }\mu\text{m}$, were used for excitation and for collection. The resulting laser spot on the sample had a diameter of $\sim 600\text{ }\mu\text{m}$ with a typical power of $\sim 100\text{ mW}$.

The samples presented in this study are by the thermal decomposition of the carb SiC substrate³. Despite the fact that these contain ~ 70 layers, simple Dirac-like electronic as the ones found in exfoliated graphene persist in these highly graphitized structure the particular rotational stacking exhibited cent graphitic planes¹⁴. Dirac Fermions in structures have been evidenced by magneto by magneto-transmission¹⁶ and, more recent tunnelling spectroscopy¹⁷ and by mag scattering experiments¹⁸. Apart from the terface layers which are highly doped due t transfer from the SiC substrate¹⁵, the ma, which we probe with Raman scattering, are c with densities as low as $5 \times 10^9 \text{ cm}^{-2}$ and high as $250000 \text{ cm}^{-2}(\text{V} \cdot \text{s})^{-1}$, as deduced fro transmission experiments¹⁹. MEG sample cially the highly graphitized specimens, are nous on the scale of our laser spot and c Bernal-stacked inclusions as observed thr Raman scattering experiments⁷.

Typical Raman scattering spectra of the 2D band measured at $B = 0, 10, 20$ and 30 T are present in Fig. 1. At zero field, the 2D band is observed as a symmetric feature composed of two Lorentzian components. The main contribution to this feature is centered at 2646 cm^{-1} with a full width at half maximum (FWHM) of 26 cm^{-1} and the second, weaker, component is centered at 2675 cm^{-1} with a FWHM of 31 cm^{-1} . As the magnetic field is increased, the energy of the 2D band is observed to increase, for a given excitation wavelength, with respect to the energy of the 2D band expected for exfoliated graphene. The origin of this effect, probably due to the type of stacking of the graphitic planes and the electronic interaction between these planes, is still a matter of debate^{20,21}. The origin of the double component of the 2D band feature observed in our experiment, different than the one observed in bulk graphite, is still not clear. It could be due to Bernal-stacked inclusions under the large laser spot. We note that similar line shapes have also been observed in micro-Raman scattering measurements on epitaxial graphene samples on SiC and were interpreted as revealing graphene domains with different amount of strain²². When a magnetic field is applied perpendicular to the graphene crystal plane, both of these two components show a red shift and a broadening. We present in Fig. 2 the evolution of the Raman shift and of the FWHM of both components of the 2D band with magnetic field. From $B = 0$ to 33 T, a shift of $\sim 8 \text{ cm}^{-1}$ and an increase of 20% of the FWHM is observed.

III. DISCUSSION

From the very beginning, we would like to stress that the observed effect is quite unlikely to be related to the

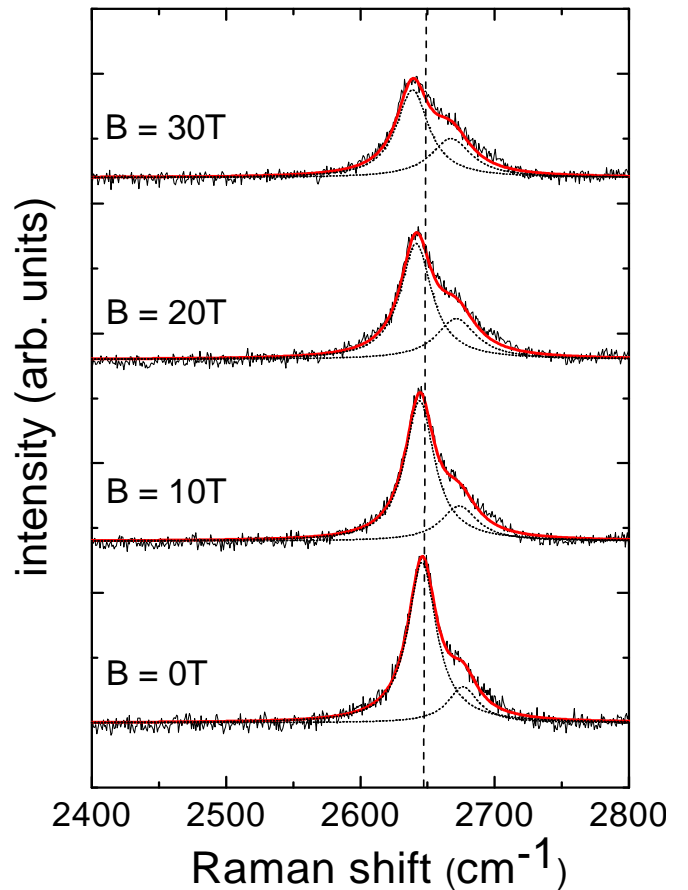


FIG. 1: (Color online) Experimental Raman scattering spectra measured at $T = 4.2$ K in the 2D band range of energy at different values of the magnetic field (black solid line), two Lorentzian fits (red solid line) and independent components of the Lorentzian fits (black dotted lines). The vertical black dashed line is a guide for the eyes.

modification of the spectrum of the emitted phonons (e. g., by electron-phonon interaction). Indeed, electrochemically top gated graphene structures allowing to tune the Fermi level up to 800 meV (carrier density up to $\sim 4 \times 10^{13} \text{ cm}^{-2}$) have been produced recently^{23,24}. Raman scattering experiments in these highly doped structures showed that the evolution of the 2D band central frequency with doping is moderate and monotonous, and can be described by a change of the equilibrium lattice parameter. Modification of the phonon dispersion due to the coupling of phonons with low energy electronic excitations across the Dirac point is noticeable near the K point of the phonon band structure (Kohn anomaly), while the phonons involved in the 2D band are too far from the K point to be affected by the Kohn anomaly. This argument remains valid even in magnetic fields used in our experiment. Indeed, the magnetic field mixes wave vectors on the scale of the inverse magnetic length, $1/l_B = \sqrt{eB/(\hbar c)} \approx 0.022 \text{ \AA}^{-1}$ at $B = 33$ T. The wave vector of the phonons responsible for the 2D peak,

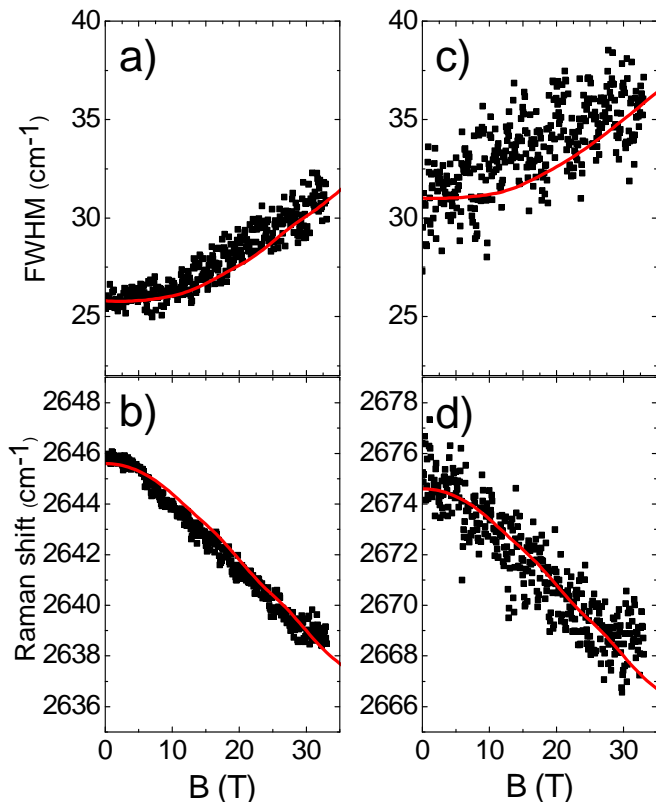


FIG. 2: (Color online) a) FWHM and b) Raman shift of the low-energy component of the $2D$ band as a function of the magnetic field. c) FWHM and d) Raman shift of the high-energy component of the $2D$ band as a function of the magnetic field. Solid red lines are calculated with our model (see text).

measured from the K point, is $q \approx 0.24 \text{ \AA}^{-1}$ at 1.7 eV excitation. Thus, $q \gg 1/l_B$ and the Kohn anomaly remains inaccessible for these phonons even at our highest fields. This is in striking contrast with the main first-order Raman feature, the so-called G band due to the doubly degenerate E_{2g} optical phonons at the Γ point of the phonon band structure. These phonons are directly in the region of the Kohn anomaly, and their frequency and lifetime are noticeably affected even by a moderate gate voltage.^{25,26} In strong magnetic fields, the G band exhibits a pronounced magneto-phonon effect,¹⁸ as the phonon state is modified by the coupling to electronic inter-Landau-level transitions.^{27,28}

In the following, we show that our observations are due to the finite curvature of the trajectories of the photo-excited electrons and holes in the magnetic field. The main idea is illustrated in Fig. 3. In the semi-classical real-space picture of the Raman process,²⁹ the incident photon creates an electron and the hole with opposite momenta at an arbitrary location within the laser spot. They subsequently propagate along the classical trajectories, and emit phonons. If they meet at some other location, again with opposite momenta, they can recom-

bine radiatively producing a scattered photon. In the absence of the magnetic field, the trajectories are straight lines, so that in order to meet at the same point with opposite momenta and contribute to the Raman scattering signal, the electron and the hole must necessarily be scattered backwards during the phonon emission.²⁹ This fixes the phonon momentum $\hbar q$ (measured from the K or K' point) as $q = p + p'$, where $\hbar p = \hbar\omega_{\text{in}}/(2v)$ and $\hbar p' = \hbar(\omega_{\text{in}} - 2\omega_{\text{ph}})/(2v)$ are the electronic momenta (also measured from the Dirac points) before and after the phonon emission, ω_{in} is the excitation frequency, ω_{ph} is the phonon frequency, and v is the electronic velocity (the slope of the Dirac cones). A slight spread in the phonon momentum due to the quantum uncertainty, $|q - p - p'| \sim 2\gamma/v$ (2γ being the electron inelastic scattering rate), gives a contribution to the width of the $2D$ peak, $\sim 2\gamma(v_{\text{ph}}/v)$, where $v_{\text{ph}} = d\omega_{\text{ph}}/dq$ is the phonon group velocity.²⁹

In a magnetic field, the electron and hole trajectories are no longer straight lines but, because of the Lorentz force that acts on charged particles in a magnetic field, they correspond to circular cyclotron orbits. As a result, one can see from Fig. 3 that (i) phonons with smaller momenta, $q = p \cos \varphi + p' \cos \varphi'$, can be emitted, and (ii) since each phonon can be emitted at an arbitrary instant in time, the length of the arc describing the electron trajectory is random [not exceeding the electron mean free path $v/(2\gamma)$], and so are the angles φ, φ' . Note that the frequencies of the two emitted phonons remain equal even with an applied magnetic field due to the symmetry under C_2 rotation around the axis perpendicular to the crystal plane.⁴⁰ Tuning the magnetic field is, in this sense, equivalent to changing the resonant conditions of the Raman scattering process at a fixed excitation wavelength and allows exploring part of the phonon band structure closer to the K point. Fact (i) results in the overall red shift of the Raman peak, while fact (ii) introduces an additional spread in q , and contributes significantly to the broadening of the peak as observed through Raman scattering measurements.

To produce the observed effects, the electron and the hole do not have to complete a full orbit. The probability of this latter event vanishes as $e^{-2\pi R(2\gamma/v)}$, where $R = p(eB/\hbar c)^{-1}$ is the cyclotron radius. This implies that the separation between the electronic Landau levels, $\hbar\omega_c = \hbar v/R$, may still be smaller than their broadening $2\hbar\gamma$ and, in our experiment, this is still the case even at $B = 30$ T. In other words, even magnetic fields far from the quantization limit can give a noticeable effect. A closely related effect has been discussed in the context of density-density response of a degenerate electron gas in a non-quantizing magnetic field³⁰.

To obtain some more quantitative information about the behavior of the $2D$ peak in magnetic fields, we calculate the Raman matrix element $\mathcal{M}(q)$ for a given phonon wave vector q in a clean graphene monolayer. It is convenient to perform the calculation in the coordinate representation, analogously to the calculation for

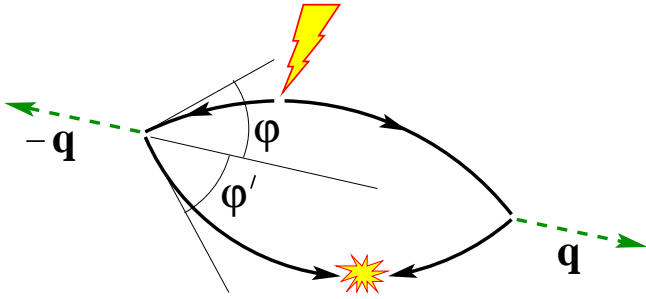


FIG. 3: (Color online) Schematic of the electron and hole motion during the Raman scattering process. The lightning represents the incident photon which creates the electron-hole pair. The solid arcs denote the propagation of the electron and the hole in the magnetic field. The flash represents the radiative recombination of the electron-hole pair. The dashed arrows denote the emitted phonons.

the D peak in the vicinity of an edge³¹ (details of this calculation are presented in the Appendix). An essential ingredient of the calculation is the semiclassical electronic Green's function for graphene in a magnetic field which was calculated in Ref. 32. Under the assumption $\omega_c \ll (\gamma, \omega_{\text{ph}}) \ll \omega_{\text{in}}$, the result of the calculation can be represented as:

$$\mathcal{M}(q) \propto \int_0^{\infty} dz \sqrt{z} e^{-[i(q-2p)+2\gamma/v]z - i[p/(12R^2)]z^3} =$$

$$= 2(i\pi)^{3/2} \frac{R}{\sqrt{p}} \frac{d}{du} [\text{Ai}^2(u) - i \text{Ai}(u) \text{Bi}(u)], \quad (1)$$

$$u \rightarrow \left(q - 2p - \frac{2i\gamma}{v} \right) \left(\frac{R^2}{p} \right)^{1/3}. \quad (2)$$

For vanishing magnetic fields, the cyclotron radius $R \rightarrow \infty$ and the relation $\mathcal{M}(q) \propto (q - 2p - 2i\gamma/v)^{3/2}$, which is Eq. (64) of Ref. 29, is recovered. For finite values of the magnetic field, the matrix element is expressed in terms of Airy functions $\text{Ai}(u)$ and $\text{Bi}(u)$ ³³. Note also the similarity with the expression for the polarization operator in Ref. 30.

Since the density of the final phonon states is practically q -independent³⁴, $|\mathcal{M}(\omega_{\text{in}}/v + \Omega/(2v_{\text{ph}}))|^2$ describes the Raman scattering intensity as a function of Ω , the Raman shift measured with respect to the center of the $2D$ peak at zero field. To illustrate the change of the peak shape in magnetic fields, we present in Fig. 4(a) $|\mathcal{M}(\omega_{\text{in}}/v + \Omega/(2v_{\text{ph}}))|^2$ for $B = 0, 10, 30$ T, considering $\hbar\omega_{\text{in}} = 1.7$ eV, $\hbar v = 7$ eV $\cdot \text{\AA}$ ($v = 1.06 \times 10^8$ cm/s), $v_{\text{ph}}/v = 50$ cm⁻¹/eV, $\hbar\gamma = 27$ meV. This value for γ is chosen in order to reproduce the observed shift of the peak maximum for increasing magnetic fields. However, the resulting FWHM for the $2D$ band is about twice smaller than the one observed experimentally at zero field. Most likely, this indicates the presence of an additional broadening mechanism besides the electronic scattering. As we cannot determine the nature of this

mechanism, we model it by introducing phenomenologically an additional broadening of the $2D$ band through a convolution of $|\mathcal{M}|^2$ with a Gaussian curve of width σ :

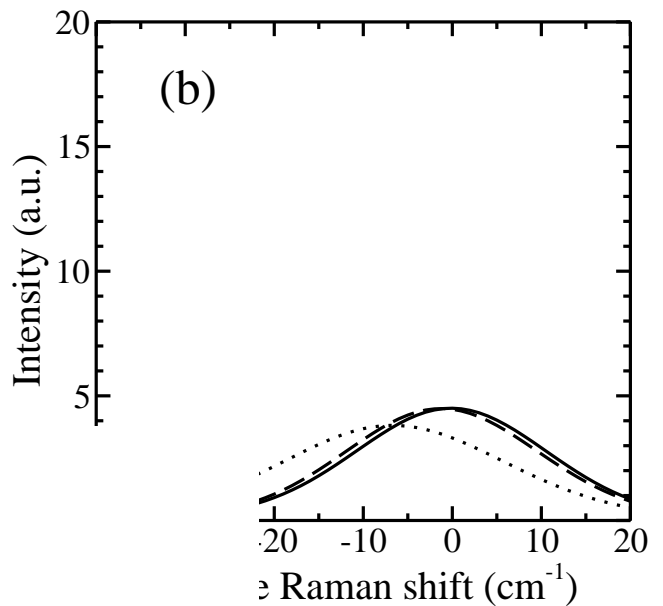
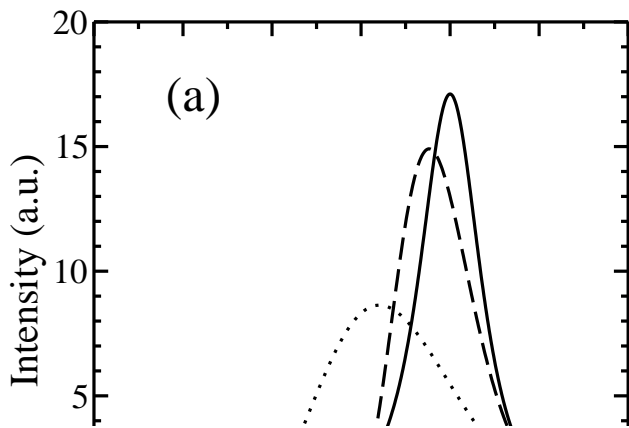
$$I_{2D}(\Omega) \propto \int_{-\infty}^{\infty} \frac{d\Omega'}{\sqrt{2\pi\sigma}} e^{-\frac{(\Omega' - \Omega)^2}{2\sigma^2}} \left| \mathcal{M} \left(\frac{\omega_{\text{in}}}{v} + \frac{\Omega'}{2v_{\text{ph}}} \right) \right|^2. \quad (3)$$

There is no simple relation between the FWHM of the original $|\mathcal{M}|^2$ peak ($8\gamma(v_{\text{ph}}/v)\sqrt{2^{2/3}-1}$ at zero field), the FWHM of the broadening Gaussian ($2\sigma\sqrt{\ln 4}$), and the FWHM of the resulting peak. The result of the convolution for $\sigma = 9.5$ cm⁻¹ is shown in Fig. 4(b).

In the following, we assume γ and σ to be independent of the magnetic field. This approximation is reasonable as long as the magnetic field is non-quantizing.³⁵ At $B = 30$ T, electrons with energy $\epsilon = 0.85$ eV measured from the Dirac point, have a cyclotron frequency $\omega_c = (v^2\hbar/\epsilon)(eB/\hbar c)$ of about 27 meV, so the strongest magnetic fields in this experiment seem to be close to the limits of validity of this approximation. Beyond this regime, Landau quantization of the electronic spectrum should manifest itself as oscillations of the peak intensity due to periodic modifications of the resonance conditions with increasing magnetic field, while in the experiment no such oscillations are observed.

The results of this calculation in terms of Raman shift and of FWHM of the peak, as described by Eq. (3), are presented as red solid lines in Fig. 2 (a)–(d) for the two components of the observed $2D$ band feature. The following parameters were adjusted: (i) the central frequencies of the two components at zero field, giving the overall vertical offset for the curves in Fig. 2 (b), (d); (ii) $\sigma = 9.5$ cm⁻¹ and $\sigma = 11.9$ cm⁻¹ were taken for the low-frequency and high-frequency components, respectively, in order to reproduce the FWHM at zero field, in combination with (iii) $\hbar\gamma = 27$ meV which determines *all four* slopes in Fig. 2 (a)–(d). Clearly, without precise knowledge of the origin of the two $2D$ band components we cannot account for the slight difference in their zero-field widths. Nevertheless, the fact that the calculation reproduces the red shift of the $2D$ band energy as a function of the magnetic field which is quadratic for fields up to 5–10 T and linear at higher fields, with a single value of γ for both components, shows that the electrons have the same dynamics in the parts of the sample, responsible for the two components.

Besides, the deduced value of $\hbar\gamma = 27$ meV is in good agreement with that deduced from the doping dependence of the $2D$ peak intensity in exfoliated graphene^{36,37} (given the energy dependence of γ and the fact that the latter measurements were performed at higher excitation energy, the electron scattering in those samples is somewhat weaker than in ours). We also note that the found value $\hbar\gamma = 27$ meV is in reasonable agreement with the line width of electronic transitions in high magnetic fields measured in this range of energy on similar samples.³⁸ This fact is remarkable because those measurements were



n^{-1} -wide Gaussian curve as given by
Raman shift is measured with respect

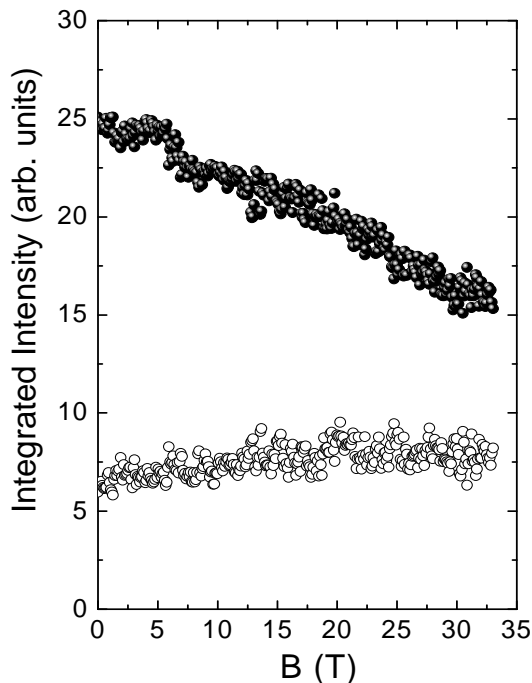


FIG. 5: Integrated intensity of the 2D band low energy component (black dots) and of the 2D band high energy component (open circles) as a function of the magnetic field.

performed in a quantizing magnetic field, and *a priori* the scattering rate does not have to be the same.³⁵

From Eq. (1) it can be seen that the integral $\int |\mathcal{M}(q)|^2 dq$ does not depend on the magnetic field. (It is sufficient to integrate over q first, and then over z ;

the magnetic field enters only through R , which drops out.) This means that under the assumption of a constant phonon density of states, the frequency-integrated intensity (the area under the peak) of the 2D band should not depend on the magnetic field. The experimental intensities for the two components are plotted on Fig. 5. Only the integrated intensity of the high-frequency component is field independent, while an overall decrease of $\sim 35\%$ of the integrated intensity of the low-frequency component is observed over the range of B between 0 and 33 T. Does it mean that the phonon density of states decreases stronger for the lower-frequency component? Again, without precise knowledge of the exact nature of the two components it is hard to give an explanation for their different behavior.

IV. CONCLUSIONS

In conclusion, we have studied, both experimentally and theoretically, the evolution of the 2D band of MEG structures in intense magnetic fields. We observe a red shift and a broadening of the 2D band as the magnetic field is increased. We have modelled this effect using a semi-classical picture in which the Lorentz force induced by the magnetic field on the photo-created electron-hole pairs, curves the carriers trajectories. This leads to a decrease of the emitted optical phonon momentum and a broadening of the 2D band as observed through Raman scattering spectroscopy. This model enables us to extract the value of the electronic scattering rate. From this we conclude that about half of the 2D band width

at zero field is due to electronic scattering while the origin of the other half remains to be clarified. Finally, we note that the observed effect of the magnetic field on the 2D peak is not specific to monolayer graphene; it should be analogous for multilayer graphene and graphite.

Acknowledgments

Part of this work has been supported by EC MTKD-CT-2005-029671, EuromagNetII, PICS-4340, ANR-08-JCJC-0034-01 and ANR-06-NANO-019 projects. P.K. is financially supported by the EU under FP7, contract no. 221515 ‘MOCNA’. M. A. thanks the Cariplo Foundation (project QUANTDEV), MICINN (Project MOSAICO) and JCYL SA052A07 for support.

Appendix A: Quasiclassical calculation of the two-phonon Raman matrix element in a uniform magnetic field

1. Classical action for a Dirac particle

The two-phonon Raman matrix element is given by a loop of four electronic Green’s functions. The latter will be taken in the quasiclassical approximation. The most important ingredient of the quasiclassical Green’s function is the classical action. Thus, we first discuss the classical action, then we give the explicit expression for the electronic Green’s function, and finally, we perform the calculation of the Raman matrix element. In fact, the first two steps have been already made by Carmier and Ullmo³², but we include them here for the sake of completeness of the presentation, and to fix the notations.

We start with the classical equation of motion of a charge in the magnetic field \mathbf{B} :

$$\frac{d\mathbf{p}}{dt} = \frac{e}{c} \mathbf{v} \times \mathbf{B} \quad (\text{A1})$$

For a Dirac electron with energy ϵ the velocity $\mathbf{v}(t) = v\mathbf{n}(t)$ and momentum $\mathbf{p}(t) = (\epsilon/v)\mathbf{n}(t)$ are expressed in terms of a unit vector, $|\mathbf{n}| = 1$. [If instead of electrons with positive and negative energies one prefers to work with positive-energy electrons and holes, then $\mathbf{p}(t) = |\epsilon/v|\mathbf{n}(t)$, so the action given below should be multiplied by $\text{sgn}\epsilon$]. Eq. (A1) can be obtained by variation of the action functional

$$S[\mathbf{r}(t)] = \int dt \left(\frac{\epsilon}{v} |\dot{\mathbf{r}}| + \frac{e}{c} \mathbf{A}(\mathbf{r}) \cdot \dot{\mathbf{r}} \right) \quad (\text{A2})$$

keeping the ends $\mathbf{r}_1, \mathbf{r}_2$ of the trajectory fixed. Indeed, upon integration by parts

$$\delta S = \int dt \left[-\frac{\epsilon}{v} \frac{d}{dt} \frac{\dot{x}_i}{|\dot{\mathbf{r}}|} + \frac{e}{c} \dot{x}_j \left(\frac{\partial A_j}{\partial x_i} - \frac{\partial A_i}{\partial x_j} \right) \right] \delta x_i + \mathbf{p}_2 \cdot \delta \mathbf{r}_2 - \mathbf{p}_1 \cdot \delta \mathbf{r}_1, \quad (\text{A3})$$

where indices $i, j = x, y, z$ label the Cartesian components, and the momentum is defined as

$$\mathbf{p} \equiv \frac{\epsilon}{v} \frac{\dot{\mathbf{r}}}{|\dot{\mathbf{r}}|} + \frac{e}{c} \mathbf{A}(\mathbf{r}). \quad (\text{A4})$$

If we now define the function $S(\mathbf{r}, \mathbf{r}')$ as the action on the classical trajectory, corresponding to the motion from \mathbf{r}' to \mathbf{r} according to Eq. (A1), we obtain $\nabla S = \mathbf{p}$ at the end of the trajectory. Thus, this function satisfies the Hamilton-Jacobi equation

$$\left| \nabla S(\mathbf{r}, \mathbf{r}') - \frac{e}{c} \mathbf{A}(\mathbf{r}) \right| = \left| -\nabla' S(\mathbf{r}, \mathbf{r}') - \frac{e}{c} \mathbf{A}(\mathbf{r}') \right| = \frac{|\epsilon|}{v}. \quad (\text{A5})$$

Also, $\partial S / \partial \epsilon$ is equal to the time it takes to go along the trajectory.

In a uniform magnetic field, \mathbf{n} is precessing with a constant frequency $\omega = -(eB/c)(v^2/\epsilon)$, and the trajectories are circles of the radius $R = v/|\omega|$. Two particular points \mathbf{r} and \mathbf{r}' can be connected either by two trajectories corresponding to short and long arcs (plus an integer number of full rotations), or by no trajectories at all if the distance between the points is greater than the circle diameter, $|\mathbf{r} - \mathbf{r}'| > 2R$. Let us assume \mathbf{B} to be along the z axis and choose the gauge $\mathbf{A}(\mathbf{r}) = (B/2)[\mathbf{e}_z \times \mathbf{r}]$. The action along the short/long arc is given by

$$S_{\pm}(\mathbf{r}, \mathbf{r}') = \frac{\epsilon R}{2v} [\vartheta_{\pm}(\mathbf{r}, \mathbf{r}') + \sin \vartheta_{\pm}(\mathbf{r}, \mathbf{r}')] - \frac{eB}{2c} [\mathbf{r} \times \mathbf{r}']_z, \quad (\text{A6})$$

$$\vartheta_+(\mathbf{r}, \mathbf{r}') = 2 \arcsin \frac{|\mathbf{r} - \mathbf{r}'|}{2R}, \quad (\text{A7})$$

$$\vartheta_-(\mathbf{r}, \mathbf{r}') = 2\pi - 2 \arcsin \frac{|\mathbf{r} - \mathbf{r}'|}{2R}. \quad (\text{A8})$$

Here $\vartheta_{\pm}(\mathbf{r}, \mathbf{r}')$ is the angular size of the short/long arc. We also introduce $\vartheta_{\pm}^{(j)}(\mathbf{r}, \mathbf{r}') = 2\pi j + \vartheta_{\pm}(\mathbf{r}, \mathbf{r}')$. We denote by \mathbf{n}_{\pm} the unit tangent vector to the short/long arc at the point \mathbf{r} (Fig. 6):

$$\mathbf{n}_{\pm}(\mathbf{r}, \mathbf{r}') = \left[\mathbf{e}_z \times \frac{\mathbf{r} - \mathbf{r}'}{|\mathbf{r} - \mathbf{r}'|} \right] \sin \frac{\vartheta_{\pm}(\mathbf{r}, \mathbf{r}')}{2} \text{sgn} \omega + \frac{\mathbf{r} - \mathbf{r}'}{|\mathbf{r} - \mathbf{r}'|} \cos \frac{\vartheta_{\pm}(\mathbf{r}, \mathbf{r}')}{2}. \quad (\text{A9})$$

The tangent determines the direction of the kinematic momentum:

$$\nabla S_{\pm}(\mathbf{r}, \mathbf{r}') - \frac{e}{c} \mathbf{A}(\mathbf{r}) = \frac{\epsilon}{v} \mathbf{n}_{\pm}(\mathbf{r}, \mathbf{r}'), \quad (\text{A10})$$

$$-\nabla' S_{\pm}(\mathbf{r}, \mathbf{r}') - \frac{e}{c} \mathbf{A}(\mathbf{r}') = -\frac{\epsilon}{v} \mathbf{n}_{\mp}(\mathbf{r}, \mathbf{r}'). \quad (\text{A11})$$

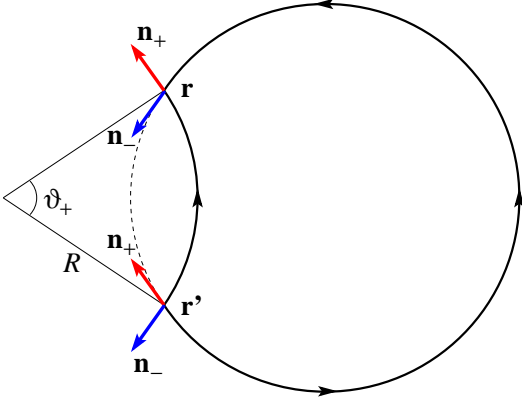


FIG. 6: (Color online) Two classical trajectories connecting the points \mathbf{r} , \mathbf{r}' .

2. Quasiclassical Green's function

Now we discuss the Green's function for the Dirac equation,

$$\left[\epsilon + i\hbar\gamma_\epsilon \text{sgn } \epsilon + v\Sigma \cdot \left(i\hbar\nabla + \frac{e}{c} \mathbf{A} \right) \right] G(\mathbf{r}, \mathbf{r}') = \mathbb{1} \delta(\mathbf{r} - \mathbf{r}'). \quad (\text{A12})$$

Here $\Sigma = (\Sigma_x, \Sigma_y)$ are the pseudospin matrices in the sublattice space, $\mathbb{1}$ is the unit matrix, and $\gamma_\epsilon > 0$ is the half of the electron or hole inelastic scattering rate, introduced phenomenologically (see Sec. IVC of Ref. 29 for the discussion of its role in Raman scattering). The factor $\text{sgn } \epsilon$ corresponds to the chronologically ordered Green's function.

The quasiclassical Green's function is represented as a sum over all trajectories of the classical motion from \mathbf{r}' to \mathbf{r} , i. e., sum over the short and long arcs, “ \pm ”, and over the number of rotations $j = 0, 1, \dots$:

$$G(\mathbf{r}, \mathbf{r}') = \sum_{j=0}^{\infty} \left[G_+^{(j)}(\mathbf{r}, \mathbf{r}') + G_-^{(j)}(\mathbf{r}, \mathbf{r}') \right], \quad (\text{A13})$$

$$\begin{aligned} G_\pm^{(j)}(\mathbf{r}, \mathbf{r}') &= e^{\pm i\pi/4} \text{sgn } \epsilon \sqrt{\frac{|\epsilon|/(\hbar v)^3}{2\pi R |\sin \vartheta_\pm^{(j)}(\mathbf{r}, \mathbf{r}')|}} \times \\ &\times \psi_{\mathbf{n}_\pm(\mathbf{r}, \mathbf{r}')} \psi_{-\mathbf{n}_\mp(\mathbf{r}, \mathbf{r}')}^\dagger e^{-i(eB/2\hbar c)[\mathbf{r} \times \mathbf{r}']_z} \times \\ &\times e^{i[\vartheta_\pm^{(j)}(\mathbf{r}, \mathbf{r}') + \sin \vartheta_\pm^{(j)}(\mathbf{r}, \mathbf{r}')]\epsilon R/(2\hbar v)} \times \\ &\times e^{-\vartheta_\pm^{(j)}(\mathbf{r}, \mathbf{r}')\gamma_\epsilon R/v}. \end{aligned} \quad (\text{A14})$$

The imaginary part of the argument of the exponential is just the classical action discussed in the previous subsection. Replacement $\epsilon \rightarrow |\epsilon|$ is required by the analytical properties of the chronologically ordered Green's function (otherwise it would correspond to the retarded Green's function). The damping factor $e^{-\gamma_\epsilon \vartheta R/v}$ is determined by the total length of the corresponding arc ϑR , including $2\pi j R$ from j full rotations. The eigenvector $\psi_{\mathbf{n}}$ of $(\mathbf{n} \cdot \Sigma)\psi_{\mathbf{n}} = \psi_{\mathbf{n}} \text{sgn } \epsilon$, $|\mathbf{n}| = 1$, can be written in terms of

the polar angle $\varphi_{\mathbf{n}}$ of the unit vector \mathbf{n} (we use the basis where Σ_x, Σ_y are represented by Pauli matrices),

$$\psi_{\mathbf{n}} = \frac{1}{\sqrt{2}} \begin{pmatrix} e^{-i\varphi_{\mathbf{n}}/2} \text{sgn } \epsilon \\ e^{i\varphi_{\mathbf{n}}/2} \end{pmatrix}. \quad (\text{A15})$$

Thus defined, $\psi_{\mathbf{n}}$ is not a single-valued function: when \mathbf{n} is rotated by 2π , $\psi_{\mathbf{n}}$ acquires a minus sign. We can fix the sign by requiring that at $\mathbf{r} \rightarrow \mathbf{r}'$, $\psi_{\mathbf{n}_+} = -\psi_{-\mathbf{n}_-} = \psi_{\mathbf{r}-\mathbf{r}'}$, $\psi_{\mathbf{n}_-} = \psi_{-\mathbf{n}_+} = \psi_{\mathbf{r}'-\mathbf{r}}$, and they evolve continuously during the motion along the circle.

We make several further remarks concerning the above expression for $G(\mathbf{r}, \mathbf{r}')$, Eqs. (A13), (A14).

(i) For $\mathbf{r} \rightarrow \mathbf{r}'$ $G(\mathbf{r}, \mathbf{r}'; \epsilon)$ reduces to the expression for the quasiclassical Green's function for $B = 0$,

$$\begin{aligned} G_0(\mathbf{r} - \mathbf{r}'; \epsilon) &= -\frac{e^{i\pi/4}}{2} \left(\mathbb{1} \text{sgn } \epsilon + \frac{\mathbf{r} - \mathbf{r}'}{|\mathbf{r} - \mathbf{r}'|} \cdot \Sigma \right) \\ &\times \sqrt{\frac{|\epsilon|/(\hbar v)^3}{2\pi |\mathbf{r} - \mathbf{r}'|}} e^{i|\epsilon|/(\hbar - \gamma_\epsilon)|\mathbf{r} - \mathbf{r}'|/v}, \end{aligned} \quad (\text{A16})$$

valid at $|\epsilon||\mathbf{r} - \mathbf{r}'|/(\hbar v) \gg 1$.

(ii) The difference between the exact Green's function and $G(\mathbf{r}, \mathbf{r}'; \epsilon)$ given by Eqs. (A13), (A14) is of higher order in \hbar . This can be checked explicitly by calculating the gradients:

$$d\varphi_{\mathbf{n}_\pm(\mathbf{r}, \mathbf{r}')} = -\frac{[\mathbf{n}_\mp \times d\mathbf{r}]_z}{R \sin \vartheta_\pm} = \frac{[\mathbf{n}_\mp \times d\mathbf{r}']_z}{R \sin \vartheta_\pm}, \quad (\text{A17})$$

$$\nabla \sin \vartheta_\pm = \frac{1}{R} \frac{\cos \vartheta_\pm}{\cos(\vartheta_\pm/2)} \frac{\mathbf{r} - \mathbf{r}'}{|\mathbf{r} - \mathbf{r}'|}, \quad (\text{A18})$$

$$\begin{aligned} \nabla \psi_{\mathbf{n}_+} &= \frac{1}{2i} \Sigma_z \psi_{\mathbf{n}_+} \nabla \varphi_{\mathbf{n}_+} \\ &= \frac{1}{2i} \Sigma_z \psi_{\mathbf{n}_+} \frac{[\mathbf{e}_z \times \mathbf{n}_-]}{R \sin \vartheta_+}, \end{aligned} \quad (\text{A19})$$

$$(\Sigma \cdot \nabla) \psi_{\mathbf{n}_+} = -\frac{(\mathbf{n}_- \cdot \Sigma) \psi_{\mathbf{n}_-}}{2R \sin \vartheta_+}, \quad (\text{A20})$$

so that at $\mathbf{r} \neq \mathbf{r}'$

$$\begin{aligned} [\epsilon + i\gamma_\epsilon \text{sgn } \epsilon + i\hbar v \Sigma \cdot \nabla] G_+^{(j)}(\mathbf{r}, \mathbf{r}'; \epsilon) &= \\ &= -\frac{i\hbar v}{R \cos^2(\vartheta_+/2)} [\mathbf{n}_+ \times \Sigma]_z G_+^{(j)}(\mathbf{r}, \mathbf{r}'; \epsilon). \end{aligned} \quad (\text{A21})$$

It is proportional to the eigenvector corresponding to the energy $-\epsilon$; thus, it can be compensated by a correction to the pre-exponential factor which does not vanish when acted upon by $\epsilon + iv\Sigma \cdot (\nabla S - ie\mathbf{A}/c)$, and thus is of the next order in \hbar :

$$\delta G_+^{(j)}(\mathbf{r}, \mathbf{r}'; \epsilon) = \frac{i\hbar v}{2\epsilon R \cos^2(\vartheta_+/2)} [\mathbf{n}_+ \times \Sigma]_z G_+^{(j)}(\mathbf{r}, \mathbf{r}'; \epsilon). \quad (\text{A22})$$

$\delta G_+^{(j)}$ is smaller than $G_+^{(j)}$ by the dimensionless parameter $\hbar v/(\epsilon R)$. However, it has a stronger divergence at

$|\mathbf{r}-\mathbf{r}'| \rightarrow 2R$; this is the manifestation of the usual breakdown of the quasiclassical approximation in the vicinity of the classical turning point.

(iii) To fix the relative phases of $G_+^{(j)}$ and $G_-^{(j)}$ we choose a given circular trajectory and consider the evolution of $G(\mathbf{r}, \mathbf{r}'; \epsilon)$ as \mathbf{r} moves along the circle. Namely, as \mathbf{r} passes the turning point at $|\mathbf{r}-\mathbf{r}'| = 2R$, $G_+^{(j)}(\mathbf{r}, \mathbf{r}'; \epsilon)$ should transform into $G_-^{(j)}(\mathbf{r}, \mathbf{r}'; \epsilon)$. In the vicinity of the turning point, $|\mathbf{r}-\mathbf{r}'| = 2R(1+z)$, $z \ll 1$, we have $\vartheta_{\pm} \approx \pi \mp \sqrt{-2z}$. Thus, ϑ_{\pm} can be viewed as two branches of the same analytical function, and $\vartheta_+ \rightarrow \vartheta_-$ when z makes a circle around $z = 0$ in the complex plane. Since $\vartheta_{\pm} + \sin \vartheta_{\pm} \approx \pi \mp (-2z)^{3/2}/6$, in order to get a decaying exponential in the classically forbidden region $|\mathbf{r}-\mathbf{r}'| > 2R$ (the positive semiaxis of z), the circle must be counterclockwise. Thus,

$$\frac{e^{i\pi/4}}{\sqrt{\sin \vartheta_+^{(j)}}} \rightarrow \frac{e^{-i\pi/4}}{\sqrt{|\sin \vartheta_-^{(j)}|}}, \quad (\text{A23})$$

precisely as in Eq. (A14).

(iv) To match the phases of $G_-^{(j)}$ and $G_+^{(j+1)}$, we consider $\mathbf{r} \rightarrow \mathbf{r}'$ and require that $G_-^{(j)}(\mathbf{r}, \mathbf{r}'; \epsilon) + G_+^{(j+1)}(\mathbf{r}, \mathbf{r}'; \epsilon)$ satisfies the homogeneous Dirac equation. Indeed, the δ -function term is produced by $G_+^{(0)}$ component, see remark (i). At $\mathbf{r} \rightarrow \mathbf{r}'$ the Green's function satisfying the homogeneous Dirac equation can be constructed in the $B \rightarrow 0$ limit. Let us introduce $\bar{G}_0(\mathbf{r}-\mathbf{r}'; \epsilon)$, the Green's function with analytical properties opposite to those of G_0 :

$$\begin{aligned} \bar{G}_0(\mathbf{r}-\mathbf{r}'; \epsilon) &= \frac{e^{-i\pi/4}}{2} \left(-\mathbb{1} \operatorname{sgn} \epsilon + \frac{\mathbf{r}-\mathbf{r}'}{|\mathbf{r}-\mathbf{r}'|} \cdot \boldsymbol{\Sigma} \right) \\ &\times \sqrt{\frac{|\epsilon|/(\hbar v)^3}{2\pi|\mathbf{r}-\mathbf{r}'|}} e^{(-i|\epsilon|/\hbar + \gamma\epsilon)|\mathbf{r}-\mathbf{r}'|/v}. \end{aligned} \quad (\text{A24})$$

It also satisfies Eq. (A12), as seen from the antisymmetry of the Dirac operator with respect to the simultaneous change $\epsilon \rightarrow -\epsilon$, $i \rightarrow -i$, $\gamma\epsilon \rightarrow -\gamma\epsilon$. Thus, $G_0(\mathbf{r}-\mathbf{r}'; \epsilon) - \bar{G}_0(\mathbf{r}-\mathbf{r}'; \epsilon)$ represents the sought solution, corresponding to the flux of particles focusing at the point \mathbf{r}' . Hence, the correspondence is $G_-^{(j)}(\mathbf{r} \rightarrow \mathbf{r}'; \epsilon) \sim -\bar{G}_0(\mathbf{r}-\mathbf{r}'; \epsilon)$ (converging wave), $G_+^{(j+1)}(\mathbf{r} \rightarrow \mathbf{r}'; \epsilon) \sim G_0(\mathbf{r}-\mathbf{r}'; \epsilon)$ (outgoing wave), which produces precisely the combination of signs as in Eq. (A14).

Remarks (iii) and (iv) can be restated in very simple terms. Upon every half-rotation $\sin \vartheta$ changes sign, so the square root produces a factor of $e^{i\pi/2}$. In addition, upon a full rotation $\psi_{\mathbf{n}}$ acquires the Berry phase $e^{i\pi}$. Hence, the sum over j in Eqs. (A13), (A14) reduces to a simple geometric progression,

$$\sum_{j=0}^{\infty} e^{j\pi(i|\epsilon|/\hbar - 2\gamma)R/v} = \frac{1}{1 - e^{\pi(i|\epsilon|/\hbar - 2\gamma)R/v}}, \quad (\text{A25})$$

which determines the poles corresponding to $\pi\epsilon R/\hbar v$ being an integer multiple of 2π , i. e., Bohr-Sommerfeld quantization rule. It gives the exact expression for the Landau levels, $|\epsilon_n/v| = \sqrt{2n|e\hbar B/c|}$.

3. Two-phonon Raman matrix element

Here we consider the matrix element $\mathcal{M}(\mathbf{q}; \varphi_{\text{in}}, \varphi_{\text{out}})$ for the transition from the initial state, corresponding to the incident photon with frequency ω_{in} polarized at the angle φ_{in} to the x axis, and no phonons, to the final state, corresponding to the scattered photon with frequency $\omega_{\text{in}} - 2\omega_{\mathbf{q}}$ polarized at the angle φ_{out} to the x axis, and two phonons with momenta $\mathbf{q}, -\mathbf{q}$ and frequencies $\omega_{\mathbf{q}}$ (\mathbf{q} is measured from the K or K' point, and for the phonons in the two valleys the frequencies $\omega_{\mathbf{q}}^{(K)} = \omega_{-\mathbf{q}}^{(K')}$ due to the time-reversal symmetry; we denote $\omega_{\mathbf{q}}^{(K)} \equiv \omega_{\mathbf{q}}$ and omit the valley index). Then, for unpolarized excitation and detection, the frequency-resolved intensity $I(\Omega)$ is given by

$$\begin{aligned} I(\Omega) &\propto \int_0^{2\pi} \frac{d\varphi_{\text{in}}}{2\pi} \frac{d\varphi_{\text{out}}}{2\pi} \int \frac{d^2\mathbf{q}}{(2\pi)^2} \\ &\times |\mathcal{M}(\mathbf{q}; \varphi_{\text{in}}, \varphi_{\text{out}})|^2 \delta(\Omega - 2\omega_{\mathbf{q}}). \end{aligned} \quad (\text{A26})$$

The matrix element is given by the loop of four Green's function with electron-photon and electron-phonon vertices (here we write it in the coordinate representation)²⁹:

$$\begin{aligned} \mathcal{M}(\mathbf{q}; \varphi_{\text{in}}, \varphi_{\text{out}}) &\propto \int \frac{d\epsilon}{2\pi} \int d^2\mathbf{r}_2 d^2\mathbf{r}_1 d^2\mathbf{r}_0 d^2\mathbf{r}'_1 \\ &\times \operatorname{Tr} \{ (\Sigma_x \cos \varphi_{\text{out}} + \Sigma_y \sin \varphi_{\text{out}}) \\ &\times G(\mathbf{r}_2, \mathbf{r}_1; \epsilon + \omega_{\text{in}}/2 - \omega_{\mathbf{q}}) \\ &\times \Sigma_z e^{-i\mathbf{q}\mathbf{r}'_1} G(\mathbf{r}_1, \mathbf{r}_0; \epsilon + \omega_{\text{in}}/2) \\ &\times (\Sigma_x \cos \varphi_{\text{in}} + \Sigma_y \sin \varphi_{\text{in}}) \\ &\times G(\mathbf{r}_0, \mathbf{r}'_1; \epsilon - \omega_{\text{in}}/2) \Sigma_z e^{i\mathbf{q}\mathbf{r}'_1} \\ &\times G(\mathbf{r}'_1, \mathbf{r}_2; \epsilon - \omega_{\text{in}}/2 + \omega_{\mathbf{q}}) \}. \end{aligned} \quad (\text{A27})$$

We will assume $\gamma\omega_{\text{in}/2}R/v \gg 1$ (non-quantizing field), then the probability of a half- or full rotation is exponentially small, and only the $G_+^{(0)}$ contribution to the Green's functions remains. The integral over ϵ is dominated by small $|\epsilon| \sim \gamma\omega_{\text{in}/2}$, so the energy arguments of the Green's functions can be assumed to have definite signs. Thus, the imaginary part of the exponent can be written as

$$\begin{aligned} &S(\mathbf{r}_2, \mathbf{r}_1; \omega_{\text{in}}/2 - \omega_{\mathbf{q}} + \epsilon) - \mathbf{q}\mathbf{r}_1 + S(\mathbf{r}_1, \mathbf{r}_0; \omega_{\text{in}}/2 + \epsilon) \\ &+ S(\mathbf{r}_0, \mathbf{r}'_1; \omega_{\text{in}}/2 - \epsilon) + \mathbf{q}\mathbf{r}'_1 \\ &+ S(\mathbf{r}'_1, \mathbf{r}_2; \omega_{\text{in}}/2 - \omega_{\mathbf{q}} + \epsilon), \end{aligned} \quad (\text{A28})$$

where the action S is that given by Eq. (A6), with the “+” subscript omitted and the energy argument explicitly introduced.

The spatial integration is performed in the stationary point approximation. Namely, in the whole 8-dimensional space $(\mathbf{r}_0, \mathbf{r}_1, \mathbf{r}'_1, \mathbf{r}_2)$ we separate a manifold on which expression (A28) is stationary. As ∇S is just the classical momentum, this manifold corresponds to joining the classical arcs connecting the pairs of points in order to satisfy momentum conservation at each point $\mathbf{r}_0, \mathbf{r}_1, \mathbf{r}'_1, \mathbf{r}_2$. Then the integration over the deviations from this manifold is performed in the Gaussian approximation, while the integration over the manifold itself has to be done more carefully. This procedure is fully analogous to that used in Sec. VIB of Ref. 31 for the edge-assisted Raman scattering.

The integration over ϵ will be performed by expanding the actions to the linear order, e. g.

$$\begin{aligned} S(\mathbf{r}_1, \mathbf{r}_0; \omega_{\text{in}}/2 + \epsilon) &\rightarrow \\ \rightarrow S(\mathbf{r}_1, \mathbf{r}_0; \omega_{\text{in}}/2) &+ \left. \frac{\partial S(\mathbf{r}_1, \mathbf{r}_0; \omega_{\text{in}}/2 + \epsilon)}{\partial \epsilon} \right|_{\epsilon=0} \epsilon, \end{aligned} \quad (\text{A29})$$

and neglecting the ϵ -dependence of the pre-exponential factors. Then the integration over ϵ gives a δ -function, $\delta(t_{01} + t_{12} - t_{21'} - t_{1'0})$, where t_{ij} is the time of travel from the point i to the point j according to the classical equations of motion. This δ -function simply expresses the fact that the electron and the hole have to travel for the same amount of time before the radiative recombination.

Let us assume the phonon momentum \mathbf{q} to be along the y axis. Out of eight spatial integration variables two correspond to translations of the trajectory as a whole. They contribute to normalization, but as we are not interested here in the overall prefactor in $\mathcal{M}(\mathbf{q})$, they can be discarded. In the remaining 6-dimensional space we introduce three coordinates y_1, φ, φ' which parametrize the stationary manifold, and three deviations $\delta x_1, \delta R, \delta R'$. The integration variables are parametrized as (see Fig. 7):

$$\begin{aligned} \mathbf{r}_0 &= \left(R \cos \varphi - \sqrt{R^2 - y_1^2}, R \sin \varphi \right) \\ &+ (\delta R \cos \varphi, \delta R \sin \varphi), \end{aligned} \quad (\text{A30})$$

$$\mathbf{r}_1 = (0, y_1) + (\delta x_1, 0), \quad (\text{A31})$$

$$\mathbf{r}'_1 = (0, -y_1) + (-\delta x_1, 0), \quad (\text{A32})$$

$$\begin{aligned} \mathbf{r}_0 &= \left(-R' \cos \varphi' - \sqrt{(R')^2 - y_1^2}, R' \sin \varphi' \right) \\ &+ (-\delta R' \cos \varphi', \delta R' \sin \varphi'), \end{aligned} \quad (\text{A33})$$

where $R = p/(eB/c)$, $R' = p'/(eB/c)$, $p = \omega_{\text{in}}/2v$, $p' = (\omega_{\text{in}} - \omega_{\mathbf{q}})/2v$. If we introduce $\varphi_1 = \arcsin(y_1/R)$, $\varphi'_1 = \arcsin(y_1/R')$, then momentum conservation reads as

$$p \sin \varphi_1 = p' \sin \varphi'_1, \quad p \cos \varphi_1 + p' \cos \varphi'_1 = q. \quad (\text{A34})$$

This ensures that the expansion of Eq. (A28) in the deviations does not have linear terms.

Now we have to expand Eq. (A28) to the second order in $\delta x_1, \delta R, \delta R'$. If we denote

$$\mathbf{s} \equiv \frac{\mathbf{r} - \mathbf{r}'}{|\mathbf{r} - \mathbf{r}'|}, \quad (\text{A35})$$

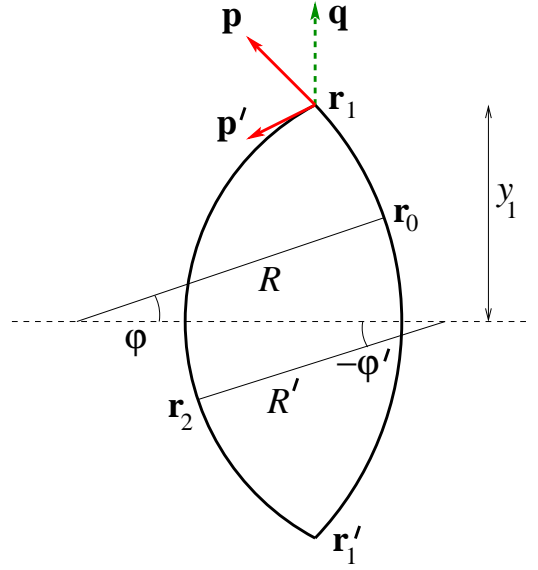


FIG. 7: (Color online) Classical trajectories determining the stationary manifold.

the second derivatives of the action can be written as

$$\begin{aligned} \frac{\partial S}{\partial x_i \partial x_j} &= \frac{\partial S}{\partial x'_i \partial x'_j} = \\ &= \frac{eB}{2c} \left[-s_i s_j \tan \frac{\vartheta_+}{2} + (\delta_{ij} - s_i s_j) \cot \frac{\vartheta_+}{2} \right], \quad (\text{A36}) \\ \frac{\partial S}{\partial x_i \partial x'_j} &= \frac{eB}{2c} \times \\ &\times \left[s_i s_j \tan \frac{\vartheta_+}{2} - (\delta_{ij} - s_i s_j) \cot \frac{\vartheta_+}{2} - e_{ijz} \right], \end{aligned} \quad (\text{A37})$$

where $e_{xyz} = -e_{yxz} = 1$, $e_{xxz} = e_{yyz} = 0$. As a result, for the quadratic part of the action ΔS we have

$$\begin{aligned} \Delta S &= -\frac{eB}{2c} \frac{\sin 2\varphi_1 (\delta R - \delta x_1 \cot \varphi_1 \sin \varphi)^2}{\sin(\varphi_1 - \varphi) \sin(\varphi_1 + \varphi)} \\ &- \frac{eB}{2c} \frac{\sin 2\varphi'_1 (\delta R' - \delta x'_1 \cot \varphi'_1 \sin \varphi')^2}{\sin(\varphi'_1 - \varphi') \sin(\varphi'_1 + \varphi')} \\ &- \frac{eB}{c} (\cot \varphi_1 + \cot \varphi'_1) (\delta x_1)^2. \end{aligned} \quad (\text{A38})$$

After integration over $\delta R, \delta R', \delta x_1$, performed in the Gaussian integration, we are left with three spatial integration variables φ, φ', y_1 , and the energy variable. As mentioned above, the latter gives the temporal δ -function,

$$\delta(t_{01} + t_{12} - t_{21'} - t_{1'0}) = \frac{v}{2} \delta(R\varphi + R'\varphi'), \quad (\text{A39})$$

which also lifts the integration over φ' . Let us take the limit $\omega_{\mathbf{q}} \ll \omega_{\text{in}}$, and neglect the difference between R and R' and between φ_1 and φ'_1 . Choosing φ_1 as the

integration variable instead of y_1 , we obtain

$$\begin{aligned} \mathcal{M}(q) \propto & \int_0^{\pi/2} R \cos \varphi_1 d\varphi_1 \int_{-\varphi_1}^{\varphi_1} d\varphi \frac{\sqrt{R \tan \varphi_1}}{\sin 2\varphi_1} \times \\ & \times e^{2ipR(\varphi_1 + \sin \varphi_1 \cos \varphi_1) - 2iqR \sin \varphi_1 - 4\gamma R \varphi_1/v} \times \\ & \times \cos^2 \varphi_1 \cos(\varphi_{\text{in}} - \varphi) \cos(\varphi_{\text{out}} - \varphi). \quad (\text{A40}) \end{aligned}$$

The first integration is simply $R \cos \varphi_1 d\varphi_1 = dy_1$, the factor $\sqrt{R \tan \varphi_1} / \sin 2\varphi_1$ comes from the gaussian integration, and the cosines give the angular dependence of the electron-photon $[\cos(\varphi_{\text{in,out}} - \varphi)]$ and electron-phonon $(\cos \varphi_1)$ matrix elements. Integration over φ gives

$$\begin{aligned} \mathcal{M}(q) \propto & \int_0^{\pi/2} R^{3/2} d\varphi_1 \sqrt{\sin \varphi_1 \cos^3 \varphi_1} \times \\ & \times e^{2ipR(\varphi_1 + \sin \varphi_1 \cos \varphi_1) - 2iqR \sin \varphi_1 - 4\gamma R \varphi_1/v} \times \\ & \times \left[\frac{\cos(\varphi_{\text{in}} - \varphi_{\text{out}})}{(\sin \varphi_1)/\varphi_1} + \cos \varphi_1 \cos(\varphi_{\text{in}} + \varphi_{\text{out}}) \right]. \quad (\text{A41}) \end{aligned}$$

Taking advantage of the limit $\gamma R/v \gg 1$, we can focus on

short arcs, so that $\varphi_1 \ll 1$ and $|2p - q| \ll p$. Thus, we expand the exponent to φ_1^3 , while in the prefactor we keep the leading term at $\varphi_1 \rightarrow 0$. In the experiment described in the paper, the excitation and detection are unpolarized, so we simply omit the the expression in the square brackets, which describes the polarization dependence. Denoting $R\varphi_1 = z$, we arrive at

$$\mathcal{M}(q) \propto \int_0^\infty dz \sqrt{z} e^{-[i(q-2p)+2\gamma/v]z - i[p/(12R^2)]z^3}, \quad (\text{A42})$$

which is Eq. (1) of the main text. The integral is calculated using the relations^{33,39}

$$\frac{1}{2\pi^{3/2}} \int_0^\infty \frac{dt}{\sqrt{t}} \cos\left(xt + \frac{t^3}{12} + \frac{\pi}{4}\right) = \text{Ai}^2(x), \quad (\text{A43})$$

$$\frac{1}{2\pi^{3/2}} \int_0^\infty \frac{dt}{\sqrt{t}} \sin\left(xt + \frac{t^3}{12} + \frac{\pi}{4}\right) = \text{Ai}(x) \text{Bi}(x) \quad (\text{A44})$$

-
- ¹ A.K. Geim, and K.S. Novoselov, *Nature Mat.* **6**, 183, (2007)
- ² K.S. Novoselov, D. Jiang, F. Schedin, T.J. Booth, V.V. Khotkevich, S.V. Morozov, and A.K. Geim, *PNAS* **102**, 10451, (2005).
- ³ C. Berger, Z. Song, Z. Li, X. Li, A.Y. Ogbazghi, R. Feng, Z. Dai, A.N. Marchenko, E.H. Conrad, P.N. First, and W.A. de Heer, *J. Phys. Chem.* **108**, 19912, (2004).
- ⁴ P.N. Sutter, J.I. Flege, and E.A. Sutter, *Nature Mat.* **7**, 406, (2008).
- ⁵ A.C. Ferrari, J.C. Meyer, V. Scardaci, C. Casiraghi, M. Lazzeri, F. Mauri, S. Piscanec, D. Jiang, K.S. Novoselov, S. Roth, and A.K. Geim, *Phys. Rev. Lett.* **97**, 187401, (2006).
- ⁶ D. Graf, F. Molitor, K. Ensslin, C. Stampfer, A. Jungen, C. Hierold, and L. Wirtz, *NanoLett.* **7**, 238, (2007).
- ⁷ C. Faugeras, A. Nerrière, M. Potemski, A. Mahmood, E. Dujardin, C. Berger, and W.A. de Heer, *Appl. Phys. Lett.* **92**, 011914, (2008).
- ⁸ A.V. Baranov, A.N. Bekhterev, Y.S. Bobovich, and V.I. Petrov, *Opt. Spektrosk.* **62**, 1036, (1987).
- ⁹ C. Thomsen, and S. Reich, *Phys. Rev. Lett.* **85**, 5214, (2000).
- ¹⁰ J. Kürti, V. Zólyomi, A. Grüneis, and H. Kuzmany, *Phys. Rev. B* **65**, 165433, (2002).
- ¹¹ D.M. Basko, *Phys. Rev. B* **76**, 081405(R), (2007).
- ¹² R. Saito, A. Jorio, A.G. Souza Filho, G. Dresselhaus, M.S. Dresselhaus, and M.A. Pimenta, *Phys. Rev. Lett.* **88**, 027401, (2002).
- ¹³ D.L. Mafra, G. Samsonidze, L.M. Malard, D.C. Elias, J.C. Brant, F. Plentz, E.S. Alves, and M.A. Pimenta, *Phys. Rev. B* **76**, 233407, (2009).
- ¹⁴ J. Hass, F. Varchon, J.E. Millan-Otoya, M. Sprinkle, N. Sharma, W.A. de Heer, P.N. First, L. Magaud, and E.H. Conrad, *Phys. Rev. Lett.* **100**, 125504, (2008).
- ¹⁵ C. Berger, Z. Song, X. Li, X. Wu, N. Brown, C. Naud, D. Mayou, T. Li, J. Hass, A.N. Marchenko, E.H. Conrad, P.N. First, and W.A. de Heer, *Science* **312**, 1191, (2006).
- ¹⁶ M.L. Sadowski, G. Martinez, M. Potemski, C. Berger, and W.A. de Heer, *Phys. Rev. Lett.* **97**, 266405, (2006).
- ¹⁷ D.L. Miller, K.E. Kubista, G.M. Rutter, M. Ruan, W.A. de Heer, P.N. First, and J.A. Stroscio, *Science* **324**, 924, (2009).
- ¹⁸ C. Faugeras, M. Amado, P. Kossacki, M. Orlita, M. Sprinkle, C. Berger, W.A. de Heer, and M. Potemski, *Phys. Rev. Lett.* **103**, 186803, (2009).
- ¹⁹ M. Orlita, C. Faugeras, P. Plochocka, P. Neugebauer, G. Martinez, D.K. Maude, A.-L. Barra, M. Sprinkle, C. Berger, W.A. de Heer, and M. Potemski, *Phys. Rev. Lett.* **101**, 267601, (2008).
- ²⁰ Z. Ni, Y. Wang, T. Yu, Y. You, and Z. Shen, *Phys. Rev. B* **77**, 235403, (2008).
- ²¹ P. Poncharal, A. Ayari, T. Michel, and J.-L. Sauvajol, *Phys. Rev. B* **78**, 113407, (2008).
- ²² J.A. Robinson, C.P. Puls, N.E. Staley, J.P. Stitt, M.A. Fanton, K.V. Emtsev, T. Seyller, and Y. Liu, *Nano Lett.* **9**, 964, (2009).
- ²³ A. Das, S. Pisana, B. Chakraborty, S. Piscanec, S.K. Saha, U.V. Waghmare, K.S. Novoselov, H.R. Krishnamurthy, A.K. Geim, A.C. Ferrari, and A.K. Sood, *Nature Nanotech.* **3**, 210, (2008).
- ²⁴ A. Das, B. Chakraborty, S. Piscanec, S. Pisana, A.K. Sood, and A.C. Ferrari, *Phys. Rev. B* **79**, 155417, (2009).
- ²⁵ S. Pisana, M. Lazzeri, C. Casiraghi, K.S. Novoselov, A.K. Geim, A.C. Ferrari, and F. Mauri, *Nature Mat.* **6**, 198, (2007).
- ²⁶ J. Yan, Y. Zhang, P. Kim, and A. Pinczuk, *Phys. Rev. Lett.* **98**, 166802, (2007).

- ²⁷ T. Ando, J. Phys. Soc. Jpn. **76**, 024712, (2007).
- ²⁸ M.O. Goerbig, J.-N Fuchs, K. Kechedzhi, and V.I. Fal'ko, Phys. Rev. Lett. **99**, 087401, (2007).
- ²⁹ D.M. Basko, Phys. Rev. B **78**, 125418, (2008).
- ³⁰ T.A. Sedrakyan, E.G. Mishchenko, and M.E. Raikh, Phys. Rev. Lett. **99**, 036401, (2007).
- ³¹ D.M. Basko, Phys. Rev. B **79**, 205428, (2009).
- ³² P. Carmier and D. Ullmo, Phys. Rev. B **77**, 245413, (2008).
- ³³ O. Vallée and M. Soares, *Airy Functions and Applications to Physics* (World Scientific, Hackensack, 2004).
- ³⁴ In fact, the assumption of the constant phonon density of states is not necessary, since one can use the phonon dispersion in the vicinity of the K point which has been recently measured by inelastic x-ray scattering [A. Grüneis, J. Serrano, A. Bosak, M. Lazzeri, S.L. Molodtsov, L. Wirtz, C. Attaccalite, M. Krisch, A. Rubio, F. Mauri, and T. Pichler, Phys. Rev. B **80**, 085423, (2009)]. The theoretical curves in Fig. 2 were produced using this experimental dispersion. However, calculations with a constant phonon density of states lead to an almost similar result (within a few percent).
- ³⁵ Actually, the contribution to γ from electron-electron collisions does acquire a B -dependent correction due to the curvature of the electronic trajectories.³⁰ However, when the sample is not strongly doped, it is reasonable to assume that the main source of electronic scattering is the emission of phonons. The corresponding rate depends on the magnetic field through the electronic density of states. The latter develops oscillations whose amplitude is *exponentially* small for the non-quantizing field, and the effect analyzed in the paper is indeed the dominant one. For quantizing magnetic fields, the electronic density of states is dominated by Landau levels, which should then be taken into account.
- ³⁶ D.M. Basko, S. Piscanec, and A.C. Ferrari, Phys. Rev. B **80**, 165413, (2009).
- ³⁷ C. Casiraghi, Phys. Rev. B **80**, 233407 (2009).
- ³⁸ P. Plochocka, C. Faugeras, M. Orlita, M.L. Sadowski, G. Martinez, M. Potemski, M.O. Goerbig, J.-N Fuchs, C. Berger, and W.A. de Heer, Phys. Rev. Lett. **100**, 087401, (2008).
- ³⁹ W.H. Reid, Zeitschrift für Angewandte Mathematik und Physik **46**, 159, (1995).
- ⁴⁰ It is worth noticing that only the relative arrangement of the two electron trajectories and not their particular orientation with respect to the crystal axis are relevant in our consideration. This emphasizes the generality of our approach which is valid even if a specific direction for electronic momentum could be assumed to contribute to the 2D band Raman scattering signal in sp^2 carbon materials¹³.